Metamagnetic Anomalies near Dynamic Phase Transitions

P. Riego,[1,2] P. Vavassori,[1,3] and A. Berger[1]
[1]CIC nanoGUNE, E-20018 Donostia-San Sebastian, Spain
[2]Departamento de Física de la Materia Condensada, Universidad del País Vasco, UPV/EHU, E-48080 Bilbao, Spain
[3]IKERBASQUE, The Basque Foundation for Science, E-48013 Bilbao, Spain
(Received 13 June 2016; revised manuscript received 3 February 2017; published 13 March 2017)

We report the existence of anomalous metamagnetic fluctuations in the vicinity of the dynamic phase transition (DPT) that do not occur for the corresponding thermodynamic behavior of simple ferromagnets. Our results demonstrate that key characteristics associated with the DPT are qualitatively different from conventional thermodynamic phase transitions. We also provide evidence that these differences are tunable by showing that the presence of metamagnetic fluctuations and the size of the critical scaling regime depend strongly on the amplitude of the oscillating field that is driving the DPT in the first place.

DOI: 10.1103/PhysRevLett.118.117202

Dynamic order phenomena and pattern formation [1] are ubiquitous in nature, and they are determining features of such diverse fields as laser emission [2], sand dunes [3,4], brain activity [5], materials defects [6,7], complex biological systems [8,9], or self-organized criticality [10]. Correspondingly, the study of dynamic phenomena and patterns is of utmost importance, and the achievement of a general understanding relies crucially on devising and solving appropriate models. Very successful is hereby the kinetic Ising model (IM) [11–14], which despite its simplicity allows for the description of very diverse dynamic behaviors and associated transitions, such as the dynamic phase transition (DPT). Generally, this model considers a system of exchange-coupled spins being subjected to an oscillatory magnetic field $H(t)$ of amplitude H_0 and period P [15–37]. Below the Curie temperature T_c, this system can exhibit a dynamically ordered phase and an associated DPT at a critical period P_c once P becomes comparable to the system's relaxation time τ. The dynamic order parameter is hereby the period-averaged magnetization Q, whose behavior as a function of P mimics the M vs T behavior near the thermodynamic phase transition (TPT) at T_c.

Since the DPT was first reported for the kinetic IM [15], it has been the focus of many theoretical studies [16–29] and several experimental investigations [30–34]. From all these studies, the consensus emerged that the properties of the DPT are truly analogous to those of the TPT for the equilibrium IM. For instance, a time-independent bias field H_b was identified as the conjugate field of Q, an approximate equation of state was derived, and the DPT critical exponents matched those for the TPT [21–29]. Recently, however, inconsistencies were reported for simulations of systems with surfaces, for which the DPT is absent in the surface layer in contrast to comparable equilibrium systems [35–37]. Thus, previously established DPT to TPT equivalencies ought to be carefully reevaluated. For this purpose, we explore here the vicinity of the DPT point for signs of anomalous behavior, and indeed, we observe most relevant qualitative differences between the DPT and TPTs, both in experiments and computations. Therefore, our results reaffirm the need for a substantial reevaluation of our understanding of DPTs and dynamic order phenomena in general.

For our experiments, we fabricated Co films with $(10\underline{1}0)$ crystallographic surface texture, which exhibit a single in-plane magnetic easy axis to mimic IM symmetry [34]. Furthermore, the in-plane orientation makes long-range magnetostatic interactions very weak, which should make the experimental results comparable to the entirety of theoretical work on DPTs, in which magnetostatic energy contributions are neglected. A sensitive magneto-optical Kerr effect setup [34,38] was utilized to measure the magnetization response of the sample upon applying a sinusoidal magnetic field of amplitude H_0 together with a bias field H_b. By integrating the time-dependent magnetization in individual field cycles, we obtain Q for each cycle, from which we determine its average $\langle Q\rangle$, its fluctuations $\sigma_Q = \sqrt{\langle Q^2\rangle - \langle Q\rangle^2}$, and the dynamic susceptibility $\chi_Q = d\langle Q\rangle/dH_b$ for a given set of P, H_0, and H_b.

Figures 1(a)–1(c) show how the magnetization $M(t)$ vs $H(t)$ [39] evolves as P decreases for fixed H_0 and $H_b = 0$. In Fig. 1(a), $P \gg P_c$, and the $M(H)$ behavior exhibits the conventional quasistatic hysteresis loop. The (red) dashed line in Fig. 1(a) represents the dynamic order parameter Q, which is zero here because the system is in the dynamically disordered phase. By sweeping the field faster, but keeping $P > P_c$ as in Fig. 1(b), the hysteresis distorts but maintains $Q = 0$. However, for $P < P_c$ shown in Fig. 1(c), M cannot follow the field and oscillates only slightly around a nonvanishing time-averaged value $Q \neq 0$. Given that $H_b = 0$, the system has two stable trajectories representing opposite values $+|Q|$ and $-|Q|$. The effect of H_b is visible in Fig. 1(d), where we show experimental $\langle Q\rangle$ values as a

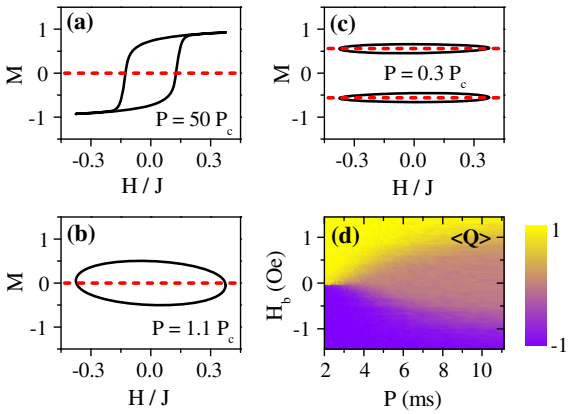

FIG. 1. (a)–(c) M vs H hysteresis loops for $H_b = 0$ and $P = 50P_c$, $1.1P_c$, and $0.3P_c$, respectively. The (red) dashed lines indicate the time-averaged values of the magnetization, i.e., the order parameter Q. (d) Experimental map of $\langle Q \rangle$ as a function of P and H_b, for $H_0 = 30.3$ Oe; the color scale is defined on the right-hand side.

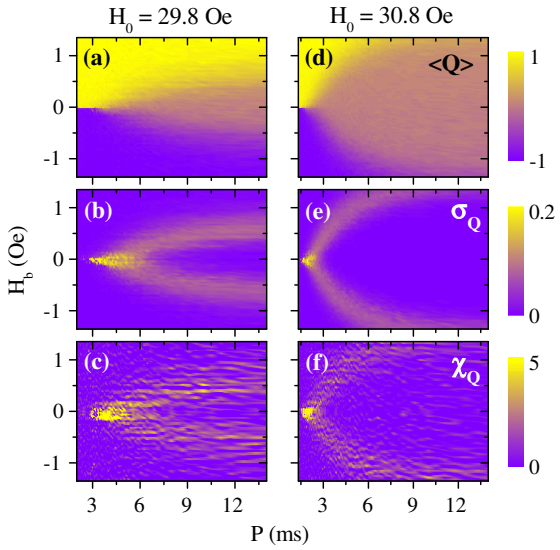

FIG. 2. (a)–(c) Experimental $\langle Q \rangle(P, H_b)$, $\sigma_Q(P, H_b)$, and $\chi_Q(P, H_b)$ maps for $H_0 = 29.8$ Oe, respectively. (d)–(f) show the same quantities for $H_0 = 30.8$ Oe. The color scale bars of $\langle Q \rangle$, σ_Q, and χ_Q are located on the right-hand side of (d), (e), and (f), respectively.

function of P and H_b for $H_0 = 30.3$ Oe. For $P < P_c = 2.6$ ms, $\langle Q \rangle$ exhibits a discontinuous change at $H_b = 0$, because the system is crossing a phase line and switches between the two stable dynamic states with $-|Q|$ and $+|Q|$ [34]. In the disordered phase, i.e., for $P > P_c$, the order parameter changes gradually, even upon inverting H_b. At first glance, the $\langle Q \rangle(P, H_b)$ map in Fig. 1(d) is analogous to the $M(T, H)$ behavior for the TPT with a ferromagnetic phase for $T < T_c$ that undergoes a first order phase transition upon inversion of H and a paramagnetic phase at $T > T_c$, where M changes gradually upon applying H. Thus, the data in Fig. 1(d) seem to support the equivalency between the DPT and a conventional TPT in a broad parameter range around the critical point.

To further explore this aspect, we measured $\langle Q \rangle$, σ_Q, and χ_Q as a function of P and H_b for different values of H_0. Figure 2 shows color-coded maps of the three quantities for $H_0 = 29.8$ Oe (left column) and $H_0 = 30.8$ Oe (right column). By comparing both columns, we observe that the position of the critical point, visible as the peak with the brightest color in the σ_Q and χ_Q maps, shifts to smaller P values as H_0 increases [40]. In addition to this expected peak at the critical point, σ_Q in Figs. 2(b) and 2(e) and χ_Q in Figs. 2(c) and 2(f) show for $P > P_c$ two sidebandlike regions with high values, which are symmetric with respect to the $H_b = 0$ line. Such sidebands representing nonmonotonic χ vs $|H|$ dependencies are not present in the vicinity of TPTs for simple ferromagnetic systems [41], and, thus, they constitute a significant qualitative difference between DPT and TPT. For TPTs of spin models, so-called Kertesz lines in the $(H - T)$-phase space are described in the literature for temperatures above T_c that are associated with an H-dependent cluster percolation, but their impact on thermodynamic quantities is weak or entirely absent [42]. So, while the here-observed χ_Q sidebands might be related to dynamic cluster percolation, their appearance and strength seem to be vastly different for the DPT if compared to TPTs.

A comparison of the sideband features for σ_Q and for χ_Q shows that they occur at the same P and H_b values, even if the susceptibility data are noisier. Thus, they appear to be in agreement with the fluctuation-dissipation relation that was reported for the DPT [19]. The elevated χ_Q values in the sidebands indicate a steep increase of the order parameter Q in a narrow H_b range for $P > P_c$. Therefore, we refer to these sidebands as metamagnetic fluctuations, in analogy to thermal equilibrium metamagnetism for which the magnetization rises sharply in a small window of applied fields. However, it is important to emphasize that $\langle Q \rangle$ remains a continuous function in the entire paramagnetic regime here. Thus, the sidebands are a change in the fluctuation characteristics and not caused by an actual phase transition.

We performed mean field approximation (MFA) calculations in order to clarify if our surprising experimental observations are related to the specifics of our material system or if they have a more general association with the DPT. Following Ref. [15], we solved the MFA equation for $M(t)$ of a spin system with nearest-neighbor exchange coupling J and spin relaxation time τ, which is subjected to an external field $H(t) = H_0 \cos[(2\pi/P)t] + H_b$ at a temperature $T < T_c$. Details of the computations are given in Ref. [40].

$Q(P, H_b)$ maps for four different H_0 values are shown in Figs. 3(a)–3(d), and the corresponding $\chi_Q(P, H_b)$ maps are displayed in Figs. 3(f)–3(i) [43]. Consistent with the DPT occurrence, all $\chi_Q(P, H_b)$ maps exhibit a dominating

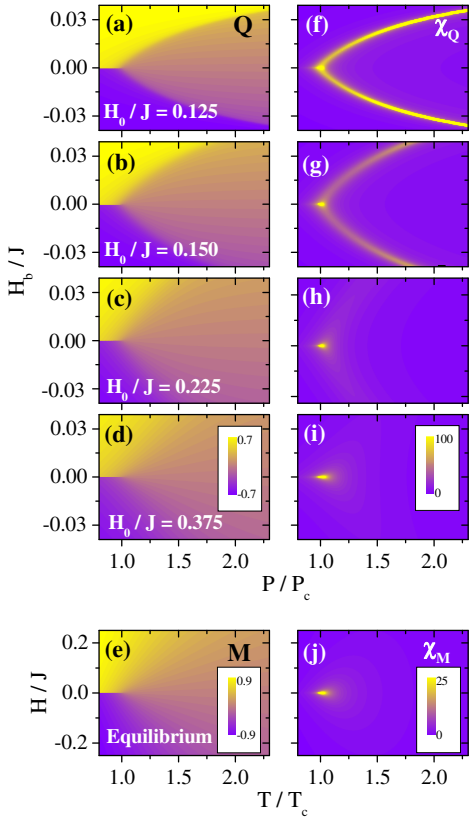

FIG. 3. (a)–(d) $Q(P, H_b)$ for different H_0 values indicated in each map; the scale bar is inside (d). (f)–(i) $\chi_Q(P, H_b)$ corresponding to maps (a)–(d), with the scale bar shown in (i). (e),(j) $M(T, H)$ and corresponding $\chi_M(T, H)$ for the TPT, each one with its corresponding scale bar inside.

central peak at the critical point ($P = P_c$, $H_b = 0$), just like the experimental data in Fig. 2. Additionally, the calculations reproduce the susceptibility sidebands, whose intensity strongly depends on H_0. The sidebands are strongest for low H_0, whereas for the largest H_0 value we calculated, $H_0/J = 0.375$, the sidebands are absent. Here, only the peak at the critical point occurs, recovering the expected simpler map for a TPT. For comparison, we computed $M(T, H)$ and the susceptibility $\chi_M(T, H) = dM/dH$ for a TPT within MFA, which are displayed in Figs. 3(e) and 3(j), respectively. χ_M shows a peak at the critical point ($T = T_c$, $H = 0$) but no secondary features in the form of sidebands. Figures 3(d) and 3(e) look essentially the same as do Figs. 3(i) and 3(j), which indicates a strong similarity of the behavior in the vicinity of the DPT and the TPT, provided that H_0 is sufficiently large, whereas for smaller H_0 values, significant differences are visible. While the high H_0 fast critical dynamics regime is experimentally not accessible, and, thus, metamagnetic fluctuations occur in all our measurements, we still find that experiments and MFA calculations show the same evolution of metamagnetic tendencies as H_0 decreases. Specifically, if one compares Figs. 2 and 3, we can see that the sidebands exhibit a decreased opening angle and increased intensities upon lowering H_0 [40].

The fact that our MFA calculations produce the same metamagnetic tendencies found in our experiments suggests that susceptibility sidebands near the DPT can be produced by a mechanism that is unrelated to percolation phenomena and the associated Kertesz lines, simply because laterally nonuniform states and, thus, percolation itself do not exist in MFA-based calculations. Therefore, we need to consider the underlying physics in more detail here. A possible origin of metamagnetic tendencies at low H_0 for the MFA case is illustrated in Fig. 4. Figure 4(a) shows the MFA equilibrium free energy F of the magnetic system under an applied field $+H_0$ (solid curve) and $-H_0$ (dashed curve). The stable state shifts with $H(t)$ and, as long as $H(t)$ is slow enough, $M(t)$ shifts symmetrically from right to left and back in a steady-state dynamic behavior. Hereby, the metastable states of antiparallel M vs H alignment in Fig. 4(a) have a significant depth, and the magnetic system exhibits a certain lifetime in them, leading to a deviation from pure sinusoidal $M(t)$ behavior visible in Fig. 4(d). When a positive H_b is now additionally applied but has a value lower than the one at which the metamagnetic onset occurs (H_b^m), F is slightly distorted, as shown in Fig. 4(b). This favors the $M > 0$ state and $M(t)$ shifts vertically, as one can see in Fig. 4(e), producing a

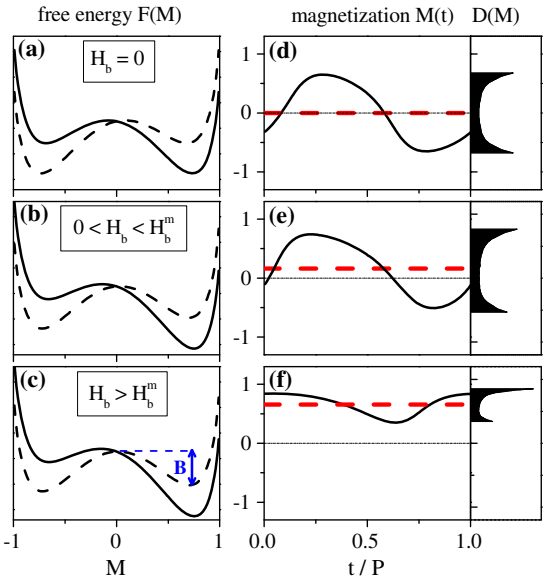

FIG. 4. (a)–(c) Low H_0 equilibrium free energy F as a function of M (based upon MFA considerations) for different H_b values indicated in the figures. Solid curves represent the $+H_0$ case and dashed curves the $-H_0$ case. The (blue) arrow in (c) indicates the energy barrier B to go from the $M > 0$ metastable state to the stable state if $-H_0$ is applied. (d)–(f) Associated M vs time behavior shown as (black) solid lines for $H_b = 0$, $0 < H_b < H_b^m$, and $H_b > H_b^m$, respectively. Horizontal (red) dashed lines represent the value of Q. The right-hand-side panels show the corresponding distributions of magnetization values $D(M)$.

small $Q > 0$ represented by the (red) dashed line. The distribution $D(M)$, which represents the probability to find the system at a magnetization value M, also shifts vertically but its shape is conserved. When H_b surpasses H_b^m as shown in Fig. 4(c), the barrier B indicated by the (blue) arrow gets so high that the system remains trapped in the $M > 0$ metastable state, even while $H(t)$ and $M(t)$ are antialigned. As a consequence, Q gets substantially larger, and $M(t)$ oscillates only slightly, leading to a compressed and asymmetric $D(M)$ as shown in Fig. 4(f). The evolution towards this metastable-state trapping happens in a rather narrow H_b range around H_b^m, producing a steep increase of Q and the corresponding peak in χ_Q. In contrast to this low H_0 case, H_b does not distort F in a substantial way for large H_0, and trapping in metastable states is not significant. Therefore, the shape of $M(t)$ is much more sinusoidal, only gradually affected by H_b, and no metamagnetic onset occurs for large H_0 [40].

It should also be mentioned that the very strong similarities between our experimental data and the results of our MFA calculations might indicate that the impact of weak long-range magnetostatic interactions is relevant in our experiments, even if it was specifically designed to have samples with very low magnetostatic interaction and even if equilibrium phase transition properties are not impacted in such samples [44]. It is, however, known that even weak long-range interactions can make magnetic properties behave mean-field-like [45].

A key consequence of this metamagnetic onset is observed in the size of the critical region. As reported in many studies, the DPT follows the same scaling laws as the TPT in the vicinity of the critical point [21–29], e.g.,

$$Q = A(P_c - P)^{\beta} \tag{1}$$

for $H_b = 0$ and P approaching P_c from below. Here, β is the critical exponent and A is a proportionality factor. In the MFA case, the critical exponent $\beta = 1/2$. However, Eq. (1) only holds in close vicinity to the critical point. We tested how close to the critical point one has to be for Eq. (1) to be valid for different H_0 values. To do so, we calculated within the MFA several data sets of Q vs P for different ranges of the reduced period $p = (P - P_c)/P_c$, namely, $-|p_{\max}| < p < |p_{\max}|$ with varying $|p_{\max}|$. We performed least-squares fits to Eq. (1) for each data set and obtained numerical values for β. Figure 5 shows the deviation of these β fit parameters from the expected MFA value as a function of $p_{\max}$, for three different values of H_0. For $H_0/J = 0.225$ the expected value is recovered in a fairly sizeable parameter range, even up to $p_{\max} = 2.5 \times 10^{-2}$, while for $H_0/J = 0.090$, one has to go as close to the critical period as $p_{\max} = 1 \times 10^{-3}$ to recover the correct $\beta = 1/2$ value even approximately. Thus, the size of the critical region, in which Eq. (1) is valid, is far smaller for the low H_0 case than in the high H_0 regime. The

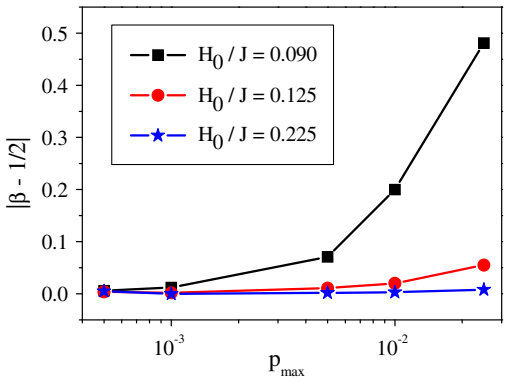

FIG. 5. Deviations of the estimated critical exponent β from the theoretical mean-field value of $1/2$ as a function of $p_{\max}$, for three different values of H_0 indicated in the legend.

universality class itself, however, is not affected for these MFA calculations, even if the range where such universality describes the actual system behavior becomes increasingly smaller. This also explains why critical exponents for the DPT have not been measured until today, because all experiments were only viable in the range of rather slow dynamics, for which the critical regime appears to be extremely small due to anomalous metamagnetic fluctuations. Correspondingly, the universality class of experimental systems has not yet been determined.

In conclusion, our results demonstrate significant anomalies in the vicinity of dynamic phase transitions, which severely limit the generally accepted broad similarities between DPTs and TPTs. We find that key characteristics associated with the DPT are qualitatively different from conventional thermodynamic phase transitions, which underlines the need for a substantial reevaluation of our understanding of dynamic phase transitions and dynamic order phenomena. Specifically, we observe a dynamically disordered phase that exhibits anomalous metamagnetic tendencies. Furthermore, we show that the scaling regime of the DPT is severely reduced in the case of slow critical dynamics, which also explains why no experimental values for critical exponents have been reported to date for the DPT.

We acknowledge support from Basque Government under Project No. PI2015_1_19 and from the Spanish Ministry of Economy and Competitiveness and the European Regional Development Fund under Project No. FIS2015-64519-R (MINECO/FEDER). P. R. acknowledges Obra Social "la Caixa" for her Ph.D. fellowship.

[1] M. C. Cross and P. C. Hohenberg, Rev. Mod. Phys. **65**, 851 (1993).

[2] J. Kröll, J. Darmo, S. S. Dhillon, X. Marcadet, M. Calligaro, C. Sirtori, and K. Unterrainer, Nature (London) **449**, 698 (2007).

[3] G. W. Baxter, R. P. Behringer, T. Fagert, and G. A. Johnson, Phys. Rev. Lett. **62**, 2825 (1989).
[4] J. L. Hansen, M. van Hecke, A. Haaning, C. Ellegaard, K. H. Andersen, T. Bohr, and T. Sams, Nature (London) **410**, 324 (2001).
[5] V. K. Jirsa and H. Haken, Phys. Rev. Lett. **77**, 960 (1996).
[6] D. Bonamy, S. Santucci, and L. Ponson, Phys. Rev. Lett. **101**, 045501 (2008).
[7] A. Shekhawat, S. Zapperi, and J. P. Sethna, Phys. Rev. Lett. **110**, 185505 (2013).
[8] I. Shmulevich, S. A. Kauffman, and M. Aldana, Proc. Natl. Acad. Sci. U.S.A. **102**, 13439 (2005).
[9] G. Schöner and J. A. S. Kelso, Science **239**, 1513 (1988).
[10] P. Bak, C. Tang, and K. Wiesenfeld, Phys. Rev. A **38**, 364 (1988).
[11] E. Stoll, K. Binder, and T. Schneider, Phys. Rev. B **8**, 3266 (1973).
[12] K. Binder, Z. Phys. **267**, 313 (1974).
[13] G. H. Fredrickson and H. C. Andersen, Phys. Rev. Lett. **53**, 1244 (1984).
[14] L. Barnett, J. T. Lizier, M. Harré, A. K. Seth, and T. Bossomaier, Phys. Rev. Lett. **111**, 177203 (2013).
[15] T. Tomé and M. J. de Oliveira, Phys. Rev. A **41**, 4251 (1990).
[16] M. Acharyya and B. K. Chakrabarti, Phys. Rev. B **52**, 6550 (1995).
[17] B. K. Chakrabarti and M. Acharyya, Rev. Mod. Phys. **71**, 847 (1999).
[18] G. Korniss, P. A. Rikvold, and M. A. Novotny, Phys. Rev. E **66**, 056127 (2002).
[19] D. T. Robb, P. A. Rikvold, A. Berger, and M. A. Novotny, Phys. Rev. E **76**, 021124 (2007).
[20] Y. Yüksel, E. Vatansever, and H. Polat, J. Phys. Condens. Matter **24**, 436004 (2012).
[21] S. W. Sides, P. A. Rikvold, and M. A. Novotny, Phys. Rev. Lett. **81**, 834 (1998).
[22] S. W. Sides, P. A. Rikvold, and M. A. Novotny, Phys. Rev. E **59**, 2710 (1999).
[23] G. Korniss, C. J. White, P. A. Rikvold, and M. A. Novotny, Phys. Rev. E **63**, 016120 (2000).
[24] H. Fujisaka, H. Tutu, and P. A. Rikvold, Phys. Rev. E **63**, 036109 (2001).
[25] G. M. Buendía and P. A. Rikvold, Phys. Rev. E **78**, 051108 (2008).
[26] H. Park and M. Pleimling, Phys. Rev. E **87**, 032145 (2013).
[27] R. A. Gallardo, O. Idigoras, P. Landeros, and A. Berger, Phys. Rev. E **86**, 051101 (2012).
[28] O. Idigoras, P. Vavassori, and A. Berger, Physica B (Amsterdam) **407**, 1377 (2012).
[29] D. T. Robb and A. Ostrander, Phys. Rev. E **89**, 022114 (2014).
[30] Y.-L. He and G.-C. Wang, Phys. Rev. Lett. **70**, 2336 (1993).
[31] Q. Jiang, H.-N. Yang, and G.-C. Wang, Phys. Rev. B **52**, 14911 (1995).
[32] Jih-Shin Suen and J. L. Erskine, Phys. Rev. Lett. **78**, 3567 (1997).
[33] D. T. Robb, Y. H. Xu, O. Hellwig, J. McCord, A. Berger, M. A. Novotny, and P. A. Rikvold, Phys. Rev. B **78**, 134422 (2008).
[34] A. Berger, O. Idigoras, and P. Vavassori, Phys. Rev. Lett. **111**, 190602 (2013).
[35] H. Park and M. Pleimling, Phys. Rev. Lett. **109**, 175703 (2012).
[36] K. Tauscher and M. Pleimling, Phys. Rev. E **89**, 022121 (2014).
[37] P. Riego and A. Berger, Phys. Rev. E **91**, 062141 (2015).
[38] J. M. Teixeira, R. Lusche, J. Ventura, R. Fermento, F. Carpinteiro, J. P. Araujo, J. B. Sousa, S. Cardoso, and P. P. Freitas, Rev. Sci. Instrum. **82**, 043902 (2011).
[39] In our numerical calculations, M is given in units of the saturation magnetization and $H(t)$ in units of the pair exchange coupling strength J.
[40] See the Supplemental Material at http://link.aps.org/supplemental/10.1103/PhysRevLett.118.117202 for further details on calculations and experimental data evaluation.
[41] More complex systems, such as layered manganites, can exhibit susceptibility sidebands due to magnetization-induced changes in the exchange coupling strength; see, for instance, A. Berger, J. F. Mitchell, D. J. Miller, and S. D. Bader, J. Appl. Phys. **89**, 6851 (2001).
[42] W. Janke, D. A. Johnston, and M. Stathakopoulos, J. Phys. A **35**, 7575 (2002).
[43] Fluctuations are suppressed in the MFA so that σ_Q cannot be calculated here. However, the experimental data show σ_Q and χ_Q to have the same qualitative behavior. Correspondingly, conclusions drawn from the study of χ_Q in MFA calculations can be extended to σ_Q in a more general theoretical framework.
[44] W. Dürr, M. Taborelli, O. Paul, R. Germar, W. Gudat, D. Pescia, and M. Landolt, Phys. Rev. Lett. **62**, 206 (1989); Yi Li and K. Baberschke, Phys. Rev. Lett. **68**, 1208 (1992).
[45] S. Miyashita, P. A. Rikvold, T. Mori, Y. Konishi, M. Nishino, and H. Tokoro, Phys. Rev. B **80**, 064414 (2009); T. Mori, S. Miyashita, and P. A. Rikvold, Phys. Rev. E **81**, 011135 (2010); T. Nakada, P. A. Rikvold, T. Mori, M. Nishino, and S. Miyashita, Phys. Rev. B **84**, 054433 (2011).